the temperature range of 40 to 77°K make it possible to determine temperature by a simple resistance measurement.

Under room temperature conditions, typical effective noise temperatures of 265°K were obtained for the assembly over a tuning range of 6.8 to 7.8 Gc/s. The amplifier alone exhibits typical effective noise temperature of 195°K at room temperature. A summary of room temperature performance follows:

Tuning range	6.8 to 7.8 Gc/s (pump-tuned)
Gain	0 to 20 dB
Bandwidth	15 Mc/s nominal
System effective noise temperature	265°K (typical)
Amplifier effective noise temperature	195°K (typical)

When the amplifier is cooled to approximately 40°K, the tuning range shifts to a range of 7.0 to 8.0 Gc/s. This shift results from mechanical changes in the amplifier body and a change in the average capacitance of the diode. After the amplifier has finished cooling, retuning is accomplished by resetting pump frequency. Nominal bandwidth of the amplifier system is unchanged by cooling. Figure 7 shows the effective noise temperature achieved as a function of signal frequency when the amplifier is cooled to 40°K. As indicated, the nominal effective noise temperature is 80°K for the system (including all input losses), and 45°K for the one-port amplifier alone. The amplifier noise temperature is approximately 20° higher than the theoretical temperature of about 25°K. In other words, the improvement is about 83 per cent of the theoretical.

Discussion and Calculations

Some interesting extrapolations of these results can be made if the effective noise contribution of each system element is considered. The system is shown schematically in Fig. 8. The effective noise temperature is given by (1) where the α's are the transmission coefficients of each lossy element, the T's are the physical temperatures of these elements, and T_{ea} is the noise temperature in °K of the amplifier at its input.

The components used in our amplifier system exhibit the following typical characteristics:

$$\alpha_1 = 0.945(-0.25\text{ dB}) \qquad T_1 = 290°K$$
$$\alpha_2 = 0.921(-0.3\text{ dB}) \qquad \overline{T}_2 = 165°K \quad (1)$$
$$\alpha_3 = 0.945(-0.25\text{ dB}) \qquad T_3 = 290°K$$

Under these conditions, the effective noise contributions (references to the input) which result from each circuit element are:

	°K
1) Input circulator (first pass)	16.89
2) Coaxial transmission line (first pass)	14.99
3) Amplifier	51.80
4) Coaxial transmission line (second pass)	1.21
5) Input circulator (second pass)	0.16
6) Output circulator-type isolator	0.17
	$T_e = 85.22$°K

The first two terms are significant contributions to the system-input excess noise temperature. These contributions and other less significant ones can be reduced appreciably by reducing the temperature of the input circulator. Typically, if the circulator temperature is reduced to 77°K, a system effective noise temperature of about 60°K should be obtained. If one assumes that further cooling of the amplifier will result in similar reductions in effective noise temperature, another useful extrapolation which is evident is the effective noise temperature one would expect to achieve by reducing the circulator temperature, and by reducing the amplifier temperature further as well. Sophisticated multiple-heat station coolers are now available which allow amplifier operation near 4.3°K and circulator operation near 77°K. If the amplifier and circulator were operated at these temperatures, a system effective noise temperature of about 13°K should be obtained. This corresponds to an amplifier noise temperature near 6°K.

Each of these changes is probably within the state of the art at present. Circulators capable of operation at 77°K have been constructed, dependable coolers for lowering the amplifier temperature to about 5°K now have become available, and amplifiers capable of operating at this temperature have been demonstrated.

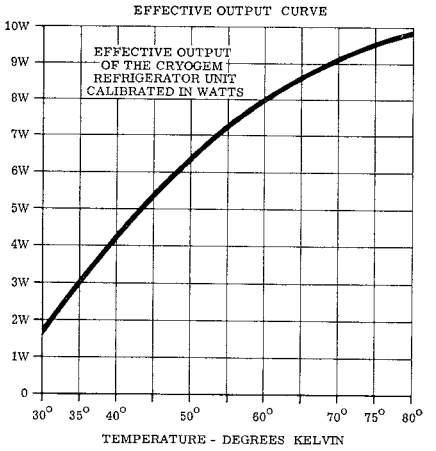

Fig. 5. Thermal load vs. temperature.

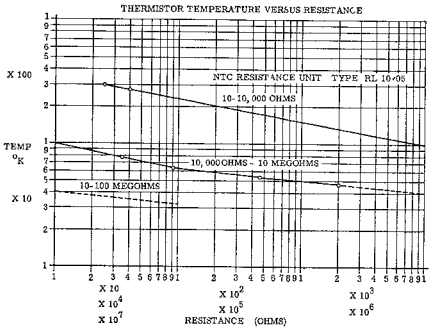

Fig. 6. Thermistor temperature as a function of resistance.

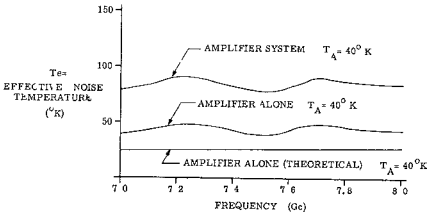

Fig. 7. System and amplifier noise temperature when amplifier is operated at 40°K.

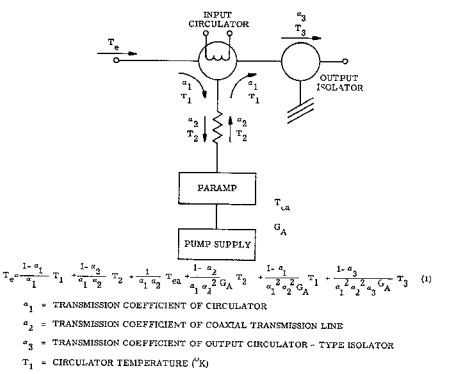

Fig. 8. Schematic diagram of system.

Conclusions

Several conclusions can be drawn from these measurements and calculations. First, an uncomplicated, closed-cycle cooled amplifier has been built and performs acceptably, yielding 83 per cent of the theoretical improvement in the system effective noise temperature. Second, logical extrapolations of the results obtained indicate that much lower system noise temperatures of about 15°K should be achievable in the 7.0 to 8.0 Gc/s frequency range by use of techniques and devices already in existence or achievable without undue effort.

C. T. Rucker
W. Morrow
E. S. Grimes, Jr.
Sperry Microwave Electronics Co.
Clearwater, Fla.

References

[1] Uenohara, M., M. Chruney, K. M. Eisele, D. C. Hanson, and A. L. Stillwell, 4-Gc parametric amplifier for satellite communication ground station receiver *Bell Sys. Tech. J.*, Jul 1963, pp 1887–1908.
[2] Blake, C., Private communications.
[3] Rucker, C. T., B. R. Savage, and E. S. Grimes, Jr., A versatile C-band cryogenic parametric amplifier presented at *1963 PTGMTT Nat'l Symp.*, Santa Monica, Calif.
[4] Blackwell, L. A , and K. L. Kotzebue, *Semiconductor Diode Parametric Amplifiers*, Englewood, N. J.: Prentice-Hall, 1961, pp 60-66.

Band-Pass Filters with Steep Skirt Selectivity

Band-pass filters exhibiting low passband insertion loss and extremely steep rejection skirts can be realized by means of

Manuscript received July 17, 1964; revised September 25, 1964. This program was supported by the NASA Goddard Space Flight Center. The work was performed while the authors were employed at Dome and Margolin, Inc., Westbury, N. Y.

resonators having more moderate values of Q than are required by conventional techniques. The design of these filters is similar to the image parameter method in that individual filter elements, each exhibiting one portion of the desired rejection, are superimposed to provide a composite characteristic. The principal difference is that the component building blocks used in our technique are filter elements designed to exhibit prescribed insertion loss characteristics.

Several direct advantages have been demonstrated by this work. These are: 1) fewer resonators may be required; 2) lower midband insertion loss can be achieved with lower Q cavities; and, 3) spurious transmissions as a result of interaction of rejecting filter sections can be avoided.

The advantages and shortcomings of the image parameter approach are well known, as are those of filters based upon low-pass exact insertion-loss prototypes of the Butterworth or Chebyshev types. Such monotonically rejecting filters have LC ladder structures, which can be readily transformed into band-pass microwave filters, and which contain many circuit elements when sharp cutoffs are required. M-derived or Chebyshev stop-band prototypes could reduce the number of elements. However, these filters are no longer simple ladder networks, and when transformed to yield band-pass or band-reject responses, they contain complex arrangements of circuit elements which cannot be readily realized as a microwave structure. This interest in band-reject filters was stimulated by the recent work done at Stanford Research Institute.

One way in which both cavity number and unloaded Q requirements may be reduced is to utilize a composite filter as shown in the upper portion of Fig. 1. A pair of band-reject filters has been used to independently set the rejection slopes. A more moderate slope band-pass (envelope) filter is used to provide rejection in the region away from the immediate vicinity of the passband. In a typical case, a Butterworth design would employ approximately 40 cavities with unloaded Q's of 35,000, where the same response could also be provided by a composite filter consisting of a seven-resonator band-pass envelope filter, and two pairs of five-resonator band-reject filters, which provide the initial slope and maintain the high rejection in the region between the slope and envelope responses. This composite filter would contain 27 resonators with unloaded Q values in the range from 7600 to 1600. These computed values of unloaded Q required for the band-reject sections were based upon the assumption that the limiting factor on unloaded Q is the peak rejection which must be attained. This is a valid assumption for moderate cutoff slope requirements.

When extremely sharp cutoff characteristics are required, a further restriction is the dissipative loss which occurs at the lower edges of the band-reject filter slope. These losses have the effect of rounding the edges of the passband response as will be shown later. In the limit, the unloaded Q required for a slope filter which has a very sharp response is determined by the permissible rounding at the passband edges. An analysis of this effect has demonstrated that optimum performance is achieved when the fewest number of resonators, required to achieve the desired rejection slope, is used. For a given available value of unloaded Q, the dissipative loss at the nominal 3-dB point is minimized and rolls off most rapidly. Thus, the optimum design for a composite filter appears to be one which uses the fewest number of resonators to achieve the desired slope, and utilizes a large number of stagger-tuned band-reject filters to achieve the rejection bandwidth. The rounding effect obviously places a lower limit upon the useable bandwidth for which a composite filter presents a more attractive approach than a band-pass filter. For filters that have moderate to wide passband bandwidth requirements with one or both extremely steep cutoff slopes, the composite filter clearly has the advantage.

In order to substantiate the composite approach, it was necessary to show that the combination of different filter sections could not produce spurious transmissions within the rejection bands. In its passband, a filter can be considered as a length of matched line. When only some sections are passing, the composite filter performance is essentially that of the rejection sections alone. When both the band-pass and band-reject filter elements are rejecting simultaneously, however, the possibility of a spurious transmission may exist. This can occur in a relatively narrow band where one attenuation slope is decreasing and the other is increasing.

The simplified equivalent circuit of Fig. 2 provides a means for evaluating this type of interaction. An arbitrary length of line is assumed to exist between the filter sections so that the effect of such phase lengths may be examined. It was found that where the phase length was a quarter-wavelength, spurious transmissions could not occur, except in the vicinity of the passband of both sections. This is a desirable effect since it assists in minimizing passband insertion loss.

In the direct-coupled case, the possibility of an extremely narrow spurious response exists. However, it has been shown that such a spurious transmission is highly attenuated by the small residual resistances present in the cavity. This dissipation was computed to be of the order of the desired rejection for the extremely narrow band-reject filters considered here. Therefore, it was concluded that proper phase lengths of interconnecting line can control the presence of spurious transmission, and those spurious transmissions which might occur would be highly attenuated. These conclusions have been confirmed experimentally.

Figure 3 is a multiple exposure oscillogram of the responses of a UHF composite filter model exicted by a swept frequency source at 400 Mc/s. Curve A is the response of the band-pass filter section alone. In curve B, a single band-reject filter section has been used to increase the steepness of the upper cutoff shirt. Curve C shows the composite response when a second band-reject cavity was stagger-tuned with the original band-reject section; reducing the 3-dB bandwidth of a band-pass filter by one-half by the addition of band-reject sections increased insertion loss by only

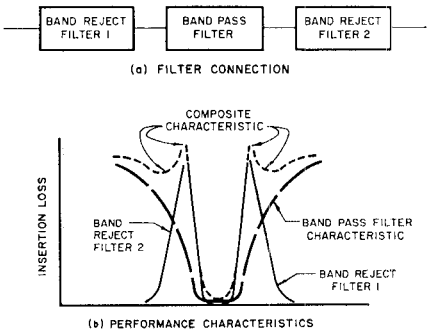

Fig. 1. Composite band-pass filter.

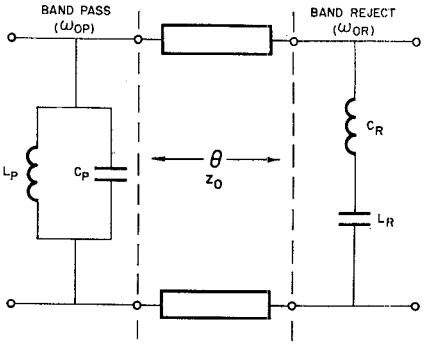

Fig. 2. Simplified equivalent circuit—composite filter analysis.

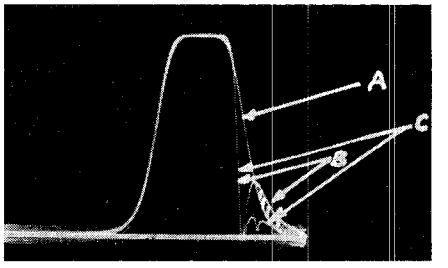

Fig. 3. UHF composite filter response. (A) Band-pass section alone. (B) Single upper skirt band reject section. (C) Two upper skirt band reject sections.

0.2 dB to 0.6 dB. Not only were the rejection skirts steeper, but a band-pass filter with the same bandwidth and Q's would have exhibited an insertion loss of at least 0.95 dB. This illustrates the moderate slope case.

The next three figures show stages in the development of a steep rejection filter at 6 Gc/s.

Figure 4 shows the individual response of a seven-cavity band-pass envelope filter as indicated by the X data points. The 3-dB to 50-dB slope is approximately 13.5 Mc/s. Superimposed on this plot is the independently measured band-pass response of a pair of tandem-connected five-cavity band-reject filters which are tuned to theoretically provide a 2 Mc/s 3-dB to 50-dB slope. The actual slope is about 4.5 Mc/s, primarily as a result of dissipation loss rounding near the band edges, and is consistent with Q's of 3000 to 4000 as realized in the slope filter resonators.

Figure 5 shows the composite response produced when the filters of the previous figure are connected in tandem, as shown schematically. Note that the slope is

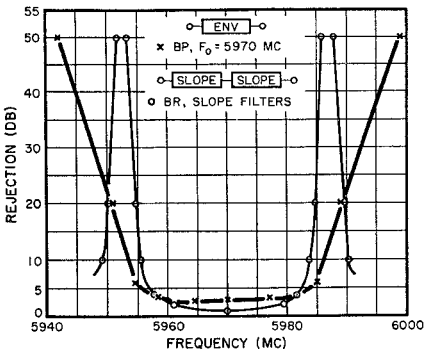

Fig. 4. Individual responses of envelope filters and pair of slope filters.

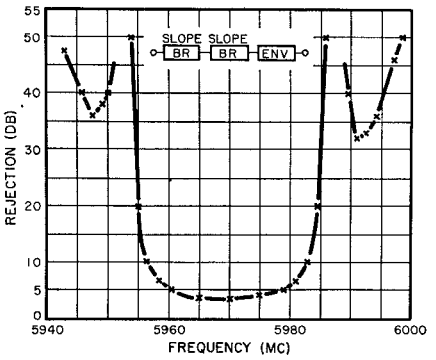

Fig. 5. Composite response of pair of slope filters and envelope filter.

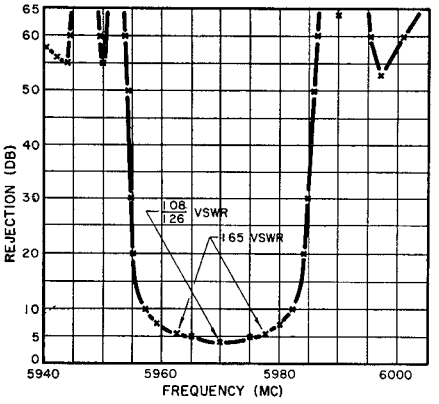

Fig. 6. Composite response—final filter.

essentially the same as that of the pair of band-reject filters of the previous figure, and also that the superposition assumption is substantiated to a high degree.

Figure 6 shows the final composite response obtained when the pair of fill-in band-reject filters is used to augment the previous response in the valley region. The slope of 5.5 Mc/s differs from the previous 4.5 Mc/s owing to the accumulated dissipation loss of the 3-dB frequency point. However, measured rejection has been increased to greater than 50dB over a broad range of frequencies on either side of the passband. Above the 10-dB level, the composite response coincides with the theoretical 2 Mc/s slope. This does not represent the optimum situation since Q's of 4000 have been used, while 9000 is readily obtainable.

Additionally it should be noted that the 27-resonator composite filter is easier to tune than an equivalent band-pass filter since band-reject resonators can be tuned independently, and the band-pass envelope filter requires only seven resonators.

ACKNOWLEDGMENT

The authors wish to thank the NASA personnel, and especially W. Allen, for advice and support during the program.

E. N. TORGOW
Rantec Corporation
Calabasas, Calif.

P. D. LUBELL
Adler Educational Systems
Div., Litton Systems, Inc.
New Rochelle, N. Y.

A New Isolator Using a Solid-State Plasma Waveguide

Nonreciprocal microwave circuits involving a tensor permeability were considered by Hogan in 1952 [1], [2], and many examples, such as isolators, circulators, modulators, switches, and phase shifters, have been developed. A gaseous plasma waveguide [3], [4] displays similar nonreciprocal properties, because of the plasma tensor permittivity in a magnetic field. The Faraday rotation and different losses for right-hand-polarized and oppositely-polarized waves lead to characteristics essentially similar to those of ferrites.

The isolator described here demonstrates the use at 24 Gc/s of a new type of electromagnetic wave [5], [6] which propagates only along one waveguide wall, determined by the propagation and external magnetic field directions. Since the theoretical upper frequency limit of the new isolator is determined by losses which appear at the cyclotron frequency, which was larger than 1000 Gc/s in the experiment described subsequently, the isolator opens the possibility of nonreciprocal devices in the mm and sub-mm wavelength region.

The properties of electromagnetic wave propagation in a solid-state plasma waveguide—for example an n-InSb bar which has been coated with copper plating—have been investigated, experimentally [5] and theoretically [6], for a plasma waveguide whose length was so large that the effect of the boundaries at the input and the output did not disturb the propagation mode. Since a short length is necessary to decrease the propagation loss for use in devices, it is also important to understand the situation for a length much shorter than the guide-wave length.

Figure 1 shows a one-dimensional model (at each quarter period of the cycle) of the propagation through a semiconductor plate whose electron mobility μ_e is so large that $\mu_e B_0 \equiv \omega_c \tau \gg 1$. Here B_0 is the external magnetic field, ω_c is the electron cyclotron frequency, τ is the electron scattering time, and the positive particles neutralizing the

Manuscript received June 19, 1964; revised August 24, 1964.

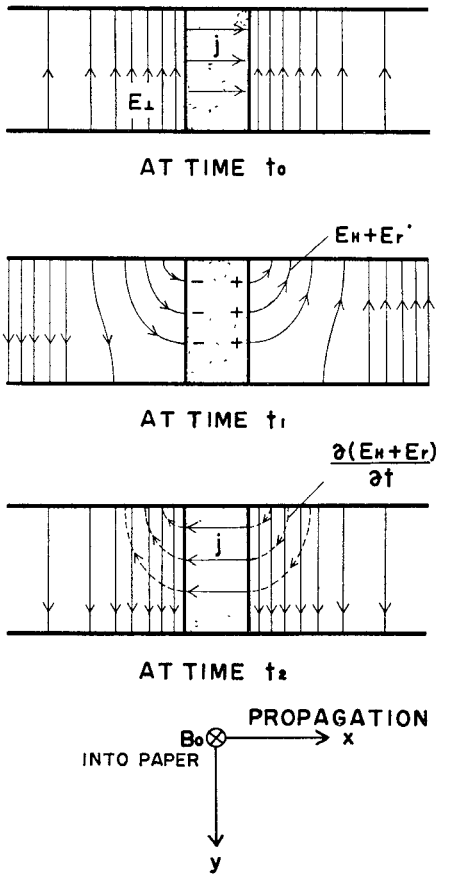

Fig. 1. Model of the propagation through a semiconductor plate in a waveguide. t_1 is one-quarter period later than t_0; t_2 is one-half period later than t_0.

electrons should be donor ions and not holes. When the electric field $E_\perp$ is maximum at the crystal at time t_0, an electron Hall current j flows in the direction perpendicular to both B_0 and E, and produces a rotational magnetic field B'. The directions of B' near the upper and lower walls are opposite so that B' adds to the magnetic field B of the normal TE mode at the upper side, and subtracts from it at the lower side. The Hall current j produces a space charge leading to a Hall field in the crystal. This "Hall" space charge and its Hall field, however, are not in the same phase as $E_\perp$, because the time constant for charging up the capacitance between the input and output boundaries is larger than the microwave period. The phase of the Hall field thus lags that of $E_\perp$ by $\pi/2$.

At time t_1, (one-quarter period later), the maximum "Hall" space charge results in an electric field equal to E_H at the outside of the crystal and the y component of E_H is reduced by $E_\perp$ near the lower wall. $B'+B$ at the upper wall is zero, and thus $\partial(B'+B)/\partial t$ is a maximum there. $\partial(B'+B)/\partial t$ produces a rotational electric field, E_r, that adds to E_H outside of the crystal but subtracts from E_H inside the crystal. Thus E_H+E_r exists only near the upper wall. At time t_2, (one-half period after t_0), E_H+E_r becomes zero and $\partial(E_H+E_r)/\partial t$ a maximum, contributing displacement current to the drift current, j.

The rotational magnetic field B'' produced by $\partial(E_H+E_r)/\partial t$ has the same effect as B', concentrating the field to the upper wall. $E_\perp$ exists in the crystal only near the upper side at t_2 because of the negative space